Stacking Disorder in Aurivillius Compounds Studied by X-Ray Diffraction Line Profile Analysis

Alexandre Boulle, Caroline Legrand, Philippe Thomas, René Guinebretière, Jean-Pierre Mercurio, Alain Dauger

Stacking Disorder in Aurivillius Compounds Studied by X-Ray Diffraction Line Profile Analysis

A. Boulle[1], C. Legrand[2], P. Thomas[2], R. Guinebretière[1], J.P. Mercurio[2] and A. Dauger[1]

[1] Science des Procédés Céramiques et des Traitements de Surface UMR 6638, ENSCI, 47-73 avenue Albert Thomas, FR-87065 Limoges Cedex, France

[2] Faculté des Sciences, Université de Limoges, 123 Av. Albert Thomas, FR-87060 Limoges Cedex, France

Keywords: Aurivillius Phase, Line Profile Analysis, X-Ray Diffraction

Abstract : $SrBi_2Nb_2O_9$ (SBN) powders and c-oriented thin films have been prepared by sol-gel process. We studied thermal behaviour of this Aurivillius compound by means of X-ray diffraction (XRD) line profile analysis. In the case of polycrystalline samples it is shown that a variation in the number of perovskite layers broadens the XRD lines similarly to stacking faults. Both 'size' and strain effects contribute to the observed width. The diffraction lines exhibited slowly decaying tails in accordance with the presence of highly localised strain fields generating almost pure 'size' broadening. For longer heat treatment the coherently diffracting domain size gradually increases and microstrains are lowered. This may be attributed to the disappearance of faults, i.e. the number of perovskite layers tends to an equilibrium value.

On epitaxial films, experiments were performed under fixed incidence and in ω-2θ scan mode. In the former situation we observed a displacement of the (00l) lines when the incidence angle was slightly changed. In ω-2θ scan mode the integral breadth reached values around 1°. When heat treatment time was increased, the width and Lorentzian content of the (00l) lines decrease attesting that stacking fault density was lowered.

1. Introduction

Since the early 90s great attention has been paid to ferroelectric thin films for non-volatile random access memories application. For this type of applications the Aurivillius compound $SrBi_2Nb_2O_9$ (SBN) is a potential candidate because of its excellent resistance to polarisation fatigue [1]. Aurivillius compounds are a family of oxides materials made of the stacking of $A_{m-1}B_mO_{3m+1}$ perovskite layers separated by Bi_2O_2 slabs (see figure 1 and ref [2]). In this type of compounds the number of perovskite blocks m lies between 1 and 5 ; for SBN it equals 2. The ferroelectric properties (e.g. polarisation and coercive field) of such compounds depend on the thickness of the perovskite layer [3]. Any disruption in the periodicity produces a loss of coherency in the diffracted beams, i.e. the peaks are broadened.

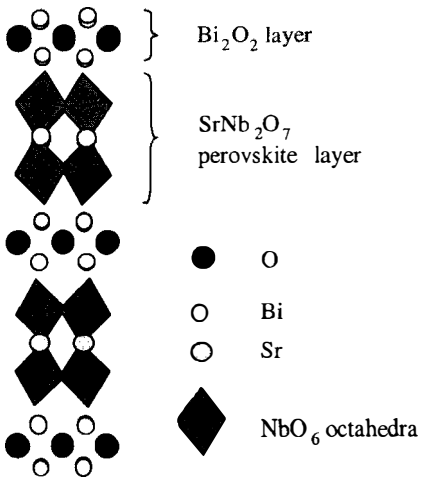

Fig. 1 : projection of the $SrBi_2Nb_2O_9$ structure along the 0x axis.

Broadening of X-ray diffraction lines arises on one hand from geometrical aberrations and radiation wavelength distribution, and on the other hand from crystalline imperfections (finite grain size, microstrains, stacking faults...) [4]. In this work we propose to study the stacking regularity of the perovskite blocks in sol-gel derived SBN by means of X-ray diffraction line

profile analysis (LPA). Both powders and c-oriented thin films are investigated. In the case of powders, the diffraction lines are strongly overlapped. One way to overcome this difficulty is to study epitaxial films so that each line is well isolated and can be easily selected by adjusting the incidence angle.

2. Experimental

2.1. Material synthesis

Appropriate SBN precursor solution was prepared first by dissolving strontium 2-ethylhexanoate in 2-ethylhexanoic acid at 120°C, subsequent addition of bismuth 2-ethylhexanoate, and finally addition of niobium ethoxide previously dissolved in ethanol.

SBN powders were obtained after conventional drying and heat treatment at 700°C for various durations (from 0.5 to 500 h). Thin films were fabricated by spinning the precursor solution at 4000 rpm for 30 s using a Sulzer photoresist spinner onto single crystalline (100) $SrTiO_3$ substrate. Details concerning the characteristics of the whole process have been published elsewhere [5].

2.2. Data collection

X-ray diffraction experiments were performed on a home made high resolution set-up [6]. This diffractometer allows the study of powders as well as polycristalline or epitaxial thin films. The primary linear beam was supplied by a rotating anode source (Brucker AXS). A Bartels four reflections monochromator, using two Ge(220) channel cut crystals provided high collimation ($\Delta\theta$ = 12") and monochromatization ($\Delta\lambda/\lambda$ = 1.4 10^{-4}) of the incident beam. Diffracted beams were collected using a curved position sensitive detector (INEL CPS120). Samples were positioned on a high precision five axis sample holder in a vacuum chamber. Sample positioning is performed by using the diffracted beams of the substrate in the case of epitaxial thin films, or of the sample holder in the case of powders [7].

Powdered specimens were studied under fixed incidence in asymmetric geometry and are continuously rotated about their surface normal during experiment. To allow precise sample positioning we used a silicon single crystal sample holder, which also permits a significant reduction of the background [8].

In order to perform LPA on oriented SBN thin films, the crystal was rocked through the Bragg law setting for a given reflection. The angular rocking range (ωmax-ωmin) was chosen wide enough to include everything from the reflection. For each incidence angle ω, diffracted beams are collected over 2θ = 120°. The final diffraction line is built up using the following equation :

$$I_{2\theta} = \int_{\omega\,\min}^{\omega\,\max} k(\omega) I_{2\theta}(\omega) d\omega \qquad \text{Eq. 1}$$

where $I_{2\theta}(\omega)$ is the intensity recorded at 2θ for the incidence angle ω ; the factor $k(\omega)$ allows for the sample absorption correction. This experiment is designated hereafter as ω-2θ scan.

2.3. Line profile analysis

After the observed line profiles are corrected for instrumental effects, the analysis of line broadening allows the determination of sample imperfections. Two approaches are used, the integral breadth method and Fourier analysis. With the latter method it is possible to obtain much more information such as column length and strain distribution.

Instrumental correction ; the breadth and shape of the instrumental profile is given by a convolution of four aberration functions : the focal spot size, equatorial divergence, spectral dispersion and detector broadening [6]. If the observed profiles are fitted with Voigt functions [9],

the integral breadth β_f of the line profiles f(x) due to sample imperfections is deduced from the breadth β_h of the observed profile and the IRF (β_g) according to [4] :

$$\beta f_L = \beta h_L - \beta g_L \qquad \text{and} \qquad \beta f_G^2 = \beta h_G^2 - \beta g_G^2 \qquad \text{Eq. 2}$$

where the subscripts L and G denotes the Lorentzian and Gaussian components.

Integral breadth method ; we follow the method introduced by Langford [9,10]. The observed profiles are assumed to be Voigtian. The Lorentzian and Gaussian components are analysed separately :

$$\beta f_L = \beta s_L + \frac{\eta_L}{2} d^* \qquad \text{and} \qquad \beta f_G^2 = \beta s_G^2 + \left(\frac{\eta_G}{2}\right)^2 d^{*2} \qquad \text{Eq. 3}$$

where the subscript s refers to the size contribution to line breadth and d* is the diffraction vector modulus. βs_L, βs_G and η_L, η_G are combined [10] and give respectively a measure of the volume averaged domain size $\langle D \rangle_v$ and apparent strain η.

Fourier analysis ; because of the large line overlapping, the Warren-Averbach method [11] is applied to the Fourier coefficients of the Voigt function modelling the f profile. The size coefficient As(L) and the mean squared strain $\langle e^2(L) \rangle$ can be separated by means of equation [12] :

$$A(L,d^*) = As(L)\left(1 - 2\pi^2 d^{*2} L^2 \left\langle e^2(L) \right\rangle\right) \qquad \text{Eq. 4}$$

where L is the correlation length and d^* the diffraction vector modulus.

All multiple line methods require at least 2 orders of reflection. In the case of SBN powders, the number of observable (00l) reflections lies between 3 and 5 over a 50° 2θ range depending on the relative intensities and the degree of line overlap. Hence, even though those lines are of rather weak intensity and often strongly overlapped, relative satisfactory results can be extracted.

3. Results and discussion

3.1. SBN powders

In figure 2 we present the XRD diagram of a powder heated 10h at 700 °C. All peaks were indexed in the orthorhombic phase (space group $A2_1am$) of SBN (JCPDS 86-1190). The orthorhombic distortion is very small since a/b equals 1.00063. The 2θ difference between the (h00) and (0k0) lines is smaller than 0.001°. Hence those lines were treated as a single peak [13,14].

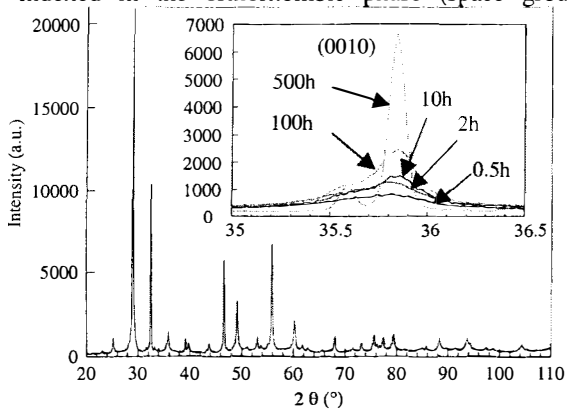

Fig. 2 : XRD diagram of the SBN phase. The sample was heat treated 10h at 700°C.

The first stage in LPA is to compare the breadth of the observed profiles h(x) with the IRF [10]. It is clear from figure 3 that the sample contribution to line broadening is significant. Moreover, the strong scatter for the β_h data seems to indicate a marked hkl-dependence.

To ascertain if the breadth effectively depend on the diffraction vector, we plotted β_f as a function of d^* in a Williamson-Hall plot [15] for the (00l) and (h00) reflections (see figure 4). The βf line for the (00l) reflection has non zero intercept and slope, indicating a marked size effect and the presence of microstrains. For the (h00) line, the intercept is almost nil (i.e. no size broadening) and the slope is non zero. In this case calculated domain size with the Langford method yields 182(56) and 33(2) nm in the [h00] and [00l] directions respectively.

The same treatment was performed for other directions ([111], [113], [115], [117], [119])). The behaviour of the apparent size could not be related to a simple crystal shape [16]. Hence the shape of the crystallite can not account for the observed size anisotropy.

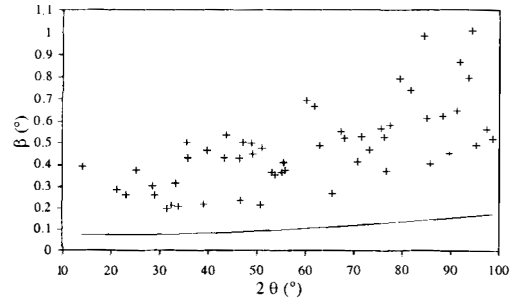

Fig. 3 : observed integral breadth (+) and IRF (—) as a function of 2θ.

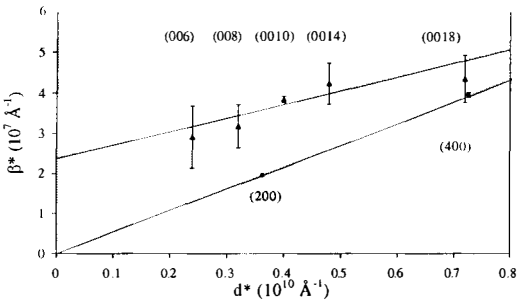

Fig. 4 : Williamson-Hall plot for the (00l) and (h00) lines.

The structure presented in figure 1 shows that perovskite blocks are stacked in the [00l] direction. Hence the difference in domain size may arise from the incorporation of stacking faults between regularly stacked layers, that is a local variation of the number m. This has been observed in similar bismuth based layered perovskites [13,14]. Those type of defects consisting of diffracting domains shifted with respect to each other, has been described by Van Berkum *et al.* as highly localised strain fields [17]. The corresponding line profiles exhibit slowly decaying tails and almost pure size broadening (i.e. order independent broadening).

Warren [11] derived the expression of the apparent domain size of a faulted crystal :

$$\frac{1}{< Dapp >_{S,V}} = \frac{1}{< D >_{S,V}} + \frac{1}{< D_F >_{S,V}} \qquad \text{Eq. 5}$$

where $<D_F>_s$ (fictious size due to faulting) is a linear combination of the faulting probabilities and depends on the hkl ; the subscripts s and v refer to surface and volume average respectively. The expression of $<D_F>_s$ has been derived for fcc, hcc and bcc structures. The second term on the right hand side of equation (5) describes the observed size anisotropy.

We are now interested in the shape of the profiles. We calculated the Voigt parameter ϕ_f (= $FWHM_f/\beta_f$) of the diffraction lines. It appeared that ϕ_f is almost order independent, so that it was possible to determine the average form factor $<\phi_f>$. The calculation yields $<\phi_f>$=0.636 and 0.754 for the (00l) and (h00) lines respectively. In other words, in the [00l] directions the profiles are purely Lorentzian, whereas they are Voigtian in the [h00] direction. This is in agreement with the presence of stacking faults since the theoretical XRD line profile of a crystal containing mistakes is approximately Lorentzian [18]. The same trend has been observed experimentally [16] and by simulation [19].

	0.5 h	2 h	10 h	100 h	500 h
$<Dapp>_s$ (nm)	11(1)	11(1)	16(1)	20(2)	98(2)
$<Dapp>_v$ (nm)	22(2)	22(2)	33(2)	40(3)	198(20)
$<e^2>^{1/2}$ (%)	0.23(8)	0.27(6)	0.17(5)	0.16(3)	0.03(1)
η (%)	0.7(5)	0.8(4)	0.5(3)	0.5(3)	0.10(6)

Table 1 : results of LPA.

When heat treatment time is increased from 0.5 to 500h the (00l) lines are becoming finer indicating domain size growth and decrease of microstrains (see inset in figure 1). The results of LPA are reported in table 1. The surf. averaged domain size $<Dapp>_s$ and $<e^2>^{1/2}$ were calculated with the Warren-Averbach method, the value of root mean squared strains was taken at $<Dapp>_s/2$ [4] ; η is the apparent strain calculated with the Langford method. Both methods gave analogous results for $<Dapp>_v$. It can be seen that

$\langle D\rangle_v = 2\langle D\rangle_s$, which corresponds to the Lorentzian limiting case [14]. The calculated volume weighted column length distribution is depicted in figure 5. The mean value of the distribution is clearly shifted towards high L values. The observed evolution may be attributed to the disappearance of stacking faults : the number of perovskite blocks tends to an equilibrium value. On the other hand, the evolution of root mean squared strain is less pronounced. This is in agreement with the previously cited model of Van Berkum.

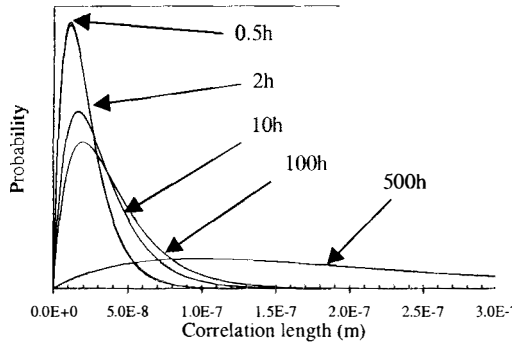

Fig. 5 : volume averaged column length distribution normalized to unit area.

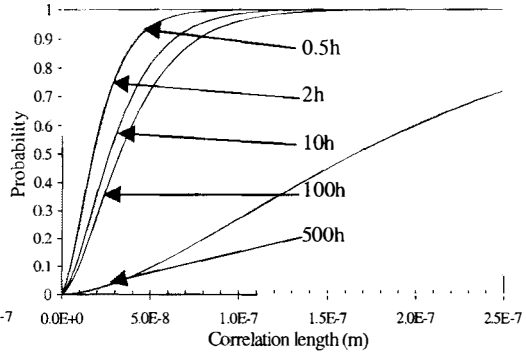

Fig. 6 : cumulative column length distribution.

According to equation (5), it is possible to calculate a fictious size $\langle D_F\rangle_v$, which can be seen as a mean distance between 2 mistakes. However, this implies the knowledge of the domain size $\langle D\rangle_v$ due to finite crystal size. According to the high cell parameter anisotropy the shape of the crystal is unlikely to be isotropic. Consequently the value of the apparent domain size in the [h00] direction can not be used as a measure of the real crystal size in the [00l]. We shall assume that an apparent size corresponding to 99% probability of the cumulative distribution (i.e. 99% of the diffracting domains are smaller than D_{max}) represent the 'real' crystal size ; hence $\langle D\rangle_v = \langle Dmax\rangle_v$. The calculation of $\langle D_F\rangle_v$ is now straightforward (see table 2). The same tendency as before is observed; the mean distance between mistakes increases, the stacking fault density is lowered. The value calculated for 500 hours is rather unrealistic. In that case we may conclude that line broadening arises only from finite grain size. In other words, stacking faults are almost non-existent.

	0.5 h	2 h	10 h	100 h	500 h
$\langle D_{max}\rangle_v$ (nm)	74(2)	75(2)	109(2)	134(3)	660(20)
$\langle D_F\rangle_v$ (nm)	31(2)	31(2)	47(2)	57(3)	282(20)

Table 2 : maximum apparent domain size (Dmax) and mean distance between mistakes (D_F)for various duration.

3.2. Thin films

In this section we present preliminary results obtained on thin films. The process described in §2.1 leads to heteroepitaxial $SrBi_2Nb_2O_9$ on $SrTiO_3$ such as $(001)_{SBN}$ // $(001)_{ST}$ and $[100]_{SBN}$ // $[110]_{ST}$ [20]. When the crystal was rocked through the Bragg law setting we observed a displacement of the (00l) lines. This corresponds to an elongated Bragg spot along the diffraction vector in reciprocal space owing to the presence of stacking faults. When samples are annealed for longer duration the range of displacement is significantly reduced.

Thin films were analysed in ω-2θ scan. Concerning the grain size and microstrains the same evolution is observed. Table 3 summarises the main results of LPA. The increase in $\langle\phi_f\rangle$

	$\langle D\rangle_v$(nm)	η (%)	$\langle\phi_f\rangle$
0.5 h	6(1)	1.2(5)	0.688
500 h	43(1)	0.29(3)	0.734

Table 3 : results of LPA on thin films.

shows that the profiles are becoming more Gaussian attesting of the disappearance of stacking faults. Since the diffraction lines are not overlapped very accurate results can be obtained. However the values are much lower than those observed for powders. The calculated domain size for a 500 hours treatment approximately equals the films thickness. Hence stacking faults have been almost completely removed.

Conclusion

The presence of stacking faults in $SrBi_2Nb_2O_9$ produces anisotropic X-ray diffraction line broadening. Moreover, the shape of the profiles in the direction of stacking are Lorentzian whereas they are Voigtian in the direction normal to the direction of stacking. Such a trend is expected from a crystal containing mistakes. $SrBi_2Nb_2O_9$ synthesised by sol-gel process contains many stacking faults. However, the mean distance between mistakes increases when the samples are thermally annealed, attesting that the stacking fault density is lowered. For a 500 hours treatment the SBN phase tends to an equilibrium state.

On thin films the same evolution is observed. However sample imperfections are much pronounced in epitaxial thin films than in powders. The effect of the interface and of limited film thickness is still under investigation. When heat treatment duration is increased the apparent domain size increases, and microstrains are lowered. The mean distance between mistakes increases and the diffraction lines are becoming more Gaussian for longer annealing, attesting of the disappearance of stacking faults. For 500 hours annealing, the samples are free of stacking faults.

References

[1] S.B. Desu, D.P. Vijay, Science 246 (1989), p. 1400
[2] B. Aurivillius, Arkiv. Kemi. 1 (1949), p. 463.
[3] X. Du, I.W. Chen, J. Am. Ceram. Soc. 81[12] (1998), p. 3260 and p. 3265.
[4] H.P. Klug, L.E. Alexander, X-ray Diffraction Procedure Procedures for Polycrystalline and Amorphous Materials (1974), New York : John Wiley.
[5] J.H. Yi, Ph. D. Thesis (1998), University of Limoges, France.
[6] O. Masson, R. Guinebretière, A. Dauger, Mater. Sci. Forum 278-281 (1998), p. 115.
[7] R. Guinebretière, A. Dauger, O. Masson, B. Soulestin, Phil. Mag. A. 79[7] (1999), p. 1517.
[8] S.T. Misture, L.R. Chattfield, R.L. Snyder, Powder Diffraction 9[3] (1994), p. 172.
[9] J.I. Langford, J. Appl. Cryst. 11 (1978), p.10.
[10] J.I. Langford, J. Res. Natl. Inst. Stand. Technol. 98 (1993), p. 321.
[11] B.E. Warren, X-ray diffraction (1969), Addison-Wesley.
[12] R. Delhez, E.J. Mittemeijer, J. Appl. Cryst. 9[3] (1976), p. 233.
[13] D. Balzar, H. Ledbetter, J. Mater. Sci. Letters 11 (1992), p. 1419.
[14] D. Balzar, J. Res. Natl. Inst. Stand. Technol. 98 (1992), p. 321.
[15] G.K. Williamson, W.H. Hall, Acta Metall. 1 (1953), p. 22.
[16] J.I. Langford, A. Boultif, J.P. Auffrédic, D. Louër, J. Appl. Cryst. 26 (1993), p. 22.
[17] J.G.M. Van Berkum, R. Delhez, Th. H. de Keijser, E.J. Mittemeijer, Acta Cryst. A52(1996), p.730.
[18] A.J.C. Wilson, X-ray Optics (1962), 2nd edition London : Methuen.
[19] C.J. Nuttall, P. Day, J. Sol. Stat. Chem. 147 (1999), p. 3.
[20] C. Legrand, J.H. Yi, P. Thomas, R. Guinebretière, J.P. Mercurio, J. Eur. Ceram. Soc. 19 (1999), p. 1379.